52nd AIAA Aerospace Sciences Meeting
13 - 17 Jan 2014
AIAA-2014-0321

Aero-Optical Mitigation of Turbulent Boundary Layers Using Large-Eddy Break-Up Devices

Adam E. Smith[1] and Stanislav Gordeyev[2]
University of Notre Dame, Notre Dame, Indiana, 46556

Results of recent experimental measurements of the effect of passive boundary layer flow control method using both single- and multiple-element Large-Eddy Break-Up devices (LEBU) on aero-optical distortions in turbulent subsonic boundary layers at a range of subsonic speeds are presented. Measurements at different locations downstream of LEBU devices were performed using a Malley probe to collect instantaneous one-dimensional wavefronts with high temporal resolution. Detailed statistical analysis of optical spectrum of aero-optical distortions are presented in order to evaluate the effect of modified turbulent structures on optical wavefront fluctuations, and to assess the mitigating aero-optical effect of each tested LEBU configuration. It was found that a long, at least 1.6 boundary-layer thicknesses, two-element LEBU device, spaced in the streamwise direction by several boundary-layer thicknesses with individual elements placed at either 0.5 or 0.6 boundary-layer thicknesses away from the wall resulted in a significant, greater than 40%, reduction in overall level of aero-optical distortions. This reduction was contributed to a suppression of the large-scale structure in the boundary layer.

I. Introduction

TURBULENT density fluctuations in the region immediately surrounding an aerodynamic vehicle, can alter the local index-of-refraction, n, as a result of the Gladstone-Dale relation, $(n-1) = K_{GD}\rho$, where ρ is the density of air and K_{GD} is the Gladstone-Dale constant [1]. This constant is a function of the wavelength of propagating light and the gas mixture of the medium [2], but for the range of visible wavelengths in air the value is approximately constant; $K_{GD} = 2.27\times10^{-4}$ m^3 kg^{-1}. From this equation, a beam of light propagating through an affected region around an aerodynamic vehicle may be distorted by the spatially- and temporally-fluctuating density fields along the path of the beam. The resulting distortions, termed aero-optic distortions [3, 4], are likely to pose a significant problem for the performance of airborne optical system, whether they are directed energy, imaging, or free-space communications applications, as disturbances to optical wavefronts in the near-field can produce considerable reductions in both time-average and instantaneous on-target intensity at a distance very far away from the aircraft [3, 4, 5].

The effect of these turbulent density fluctuations on the propagation of initially planar wavefronts can be quantified by defining the Optical Path Length (*OPL*) as the integral of the index-of-refraction, n, along the physical distance traversed by a ray of light. The resulting deviation from the average *OPL* can then be expressed as the Optical Path Difference (*OPD*), $OPD(\vec{x},t) = OPL(\vec{x},t) - \overline{OPL(\vec{x},t)}$, where the overbar denotes spatial averaging. It can be shown that *OPD* is in fact the conjugate of the zero-mean wavefront, $W(\vec{x},t) = -OPD(\vec{x},t)$. The level of wavefront aberrations is typically quantified as the time-averaged root-mean-square of *OPD* over the aperture, OPD_{rms}.

Recent research investigating the characteristics of aero-optic aberrations has included studies on turbulent boundary layers, free shear layers, tip vortices, and flows around cylindrical and hemispherical turrets [3,4]. Both experimental [6] and computational [7, 8] research has focused on characterizing the aero-optical effects of turbulent boundary layers (TBLs). Gordeyev et al [6] investigated the relationship between OPD_{rms} and flow characteristics including a Mach number, M, a boundary layer thickness, δ, and an angle of beam incidence, β, and derived useful scaling laws. Cress [9, 10] also investigated the effects of non-adiabatic wall temperature, T_w, with full wall heating experiments, and the results of these investigations were incorporated into existing scaling relationships [6, 10]. Smith & Gordeyev [11] further explored the effects of non-adiabatic wall temperature with partial wall cooling

[1] Graduate Student, Department of Mechanical and Aerospace Engineering, Hessert Laboratory for Aerospace Research, Notre Dame, IN 46556, Student Member.
[2] Research Associate Professor, Department of Mechanical and Aerospace Engineering, Hessert Laboratory for Aerospace Research, Notre Dame, IN 46556, AIAA Associate Fellow.

experiments. Results from a number of these studies showed that optically active structures within the subsonic boundary layer convect at approximately $0.82U_\infty$, which suggests that the most optically active structures in the TBL are located in the outer region, away from the wall [6]. These experimental results are supported by computational investigations of aero-optic aberrations of TBLs by Wang & Wang [7].

Gordeyev, et al. [5] have also investigated the implications of short, on the order of a millisecond, spikes in time-series of OPD_{rms} which have been observed in experiments with high-bandwidth wavefront sensors. These temporal increases of OPD_{rms} were shown to potentially cause instantaneous far-field intensity drop-outs which could severely reduce the performance of airborne optical systems which require sustained on-target intensity. This work in particular emphasizes the practical need to identify and optimize flow control techniques that are effective at mitigating Aero-optic aberrations caused by TBLs.

Several methods of passive flow control for TBLs have been identified as promising for achieving significant mitigation of TBL aero-optic effects. One method of aero-optic mitigation utilized full and partial wall cooling to reduce the total temperature of the boundary layer, and therefore reduce the strength of the density fluctuations across the boundary layer. Results from this experiment showed that a reduction in OPD_{rms} as high as 80% could be achieved, although this required cooling over nearly the entire boundary layer development length [11]. The second method, which this paper is concerned with, is the use of Large Eddy Breakup (LEBU) devices to directly modify large-scale, outer-region structures that are thought to be the primary contributors to aero-optic distortions caused by TBLs [12].

A. LEBU Devices for Aero-Optic Mitigation

LEBU devices generally are constructed from one or more thin plates or airfoils placed parallel to the wall inside of the turbulent boundary layer which act to break up large-scale turbulent structures in the outer portion of the TBL. Single-LEBU devices, as well as multi-LEBU (vertically stacked) and tandem-LEBU (horizontally spaced) devices, shown schematically in Figure 1, were studied intensively in 1980s and were shown to weaken the large-scale structure in the outer region of the boundary layer by reducing the turbulent intensity and the integral length scales of boundary-layer structures for significant distances, on the order of 100δ, downstream of the device [13-17]. LEBU devices were shown to reduce the local skin friction, but introduced additional drag themselves, causing them to be rejected as practical global drag reduction devices.

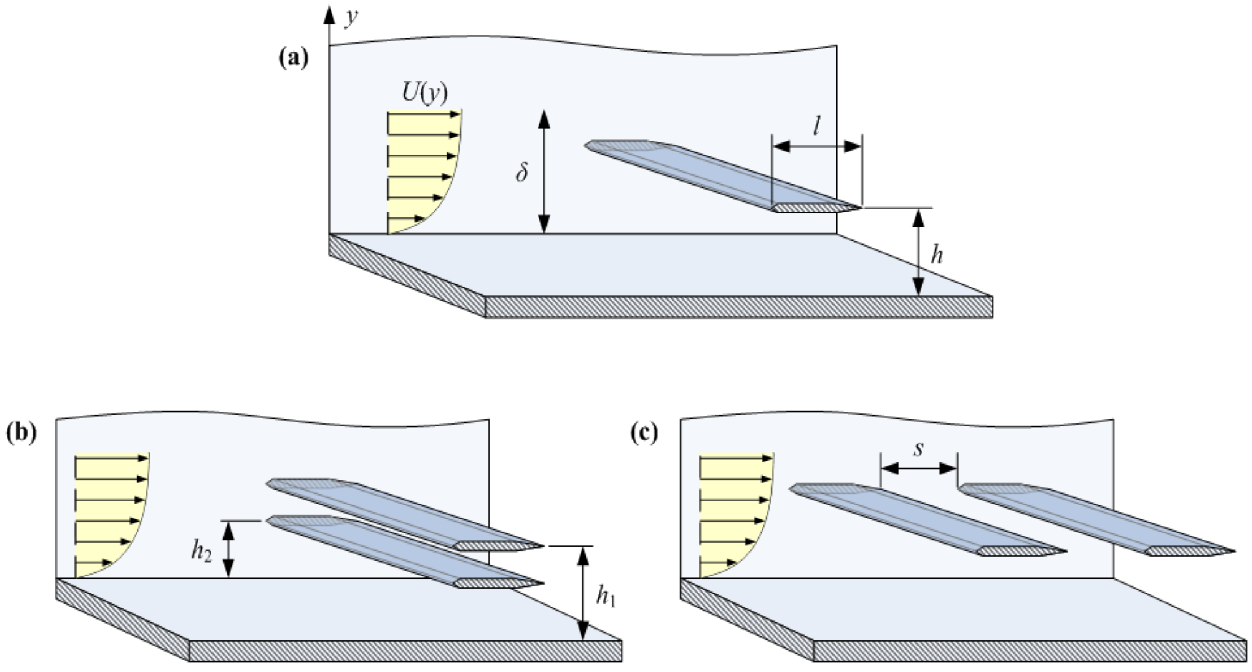

Figure 1. Schematic of (a) Single LEBU, (b) Multi-LEBU, and (c) Tandem-LEBU device configurations.

While the overall effect of LEBU devices are not substantial enough to have a net global improvements in boundary layer drag, their ability to reduce the large-scale structure was shown by Smith & Gordeyev [12] to be

effective for aero-optic flow control. Measurements of levels of aero-optic distortions, shown in Figure 2, and hot-wire velocity measurements, shown in Figure 3, in the region up to 6δ downstream of single-LEBU devices in several different configurations of device length l and height h have shown that reductions of up to approximately 30% can be achieved from suppression of large-scale turbulent structures in the outer region of the boundary layer. In addition, the aero-optic characterization of the LEBU device for some configurations suggested that, beyond 6δ in the streamwise direction, there may be an additional reduction in OPD_{rms} beyond what has been observed.

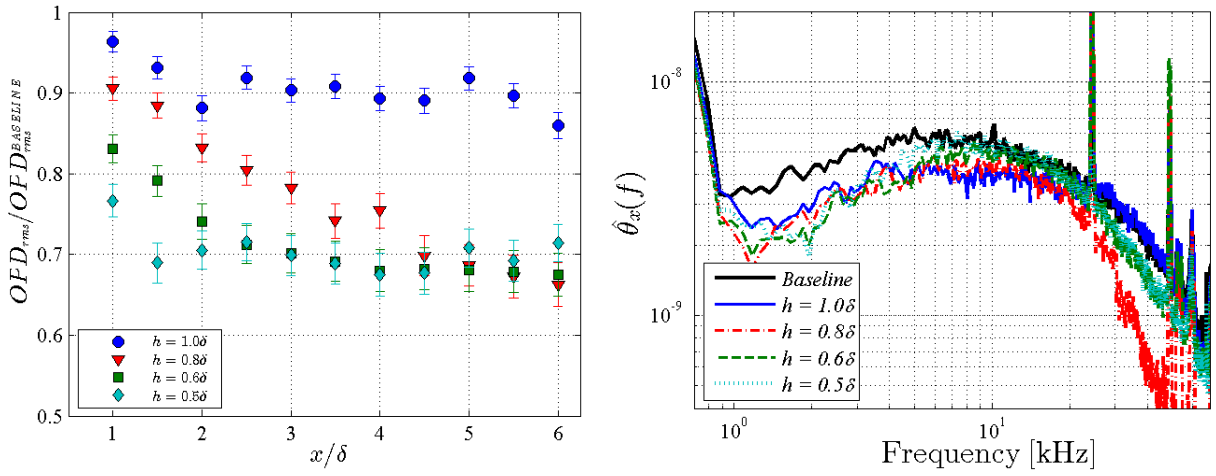

Figure 2. Comparison of streamwise OPD_{rms} variation (left) and deflection angle spectra at $x = 5.6\delta$ for different LEBU device heights (left), $l = 1.6\delta$. From [12].

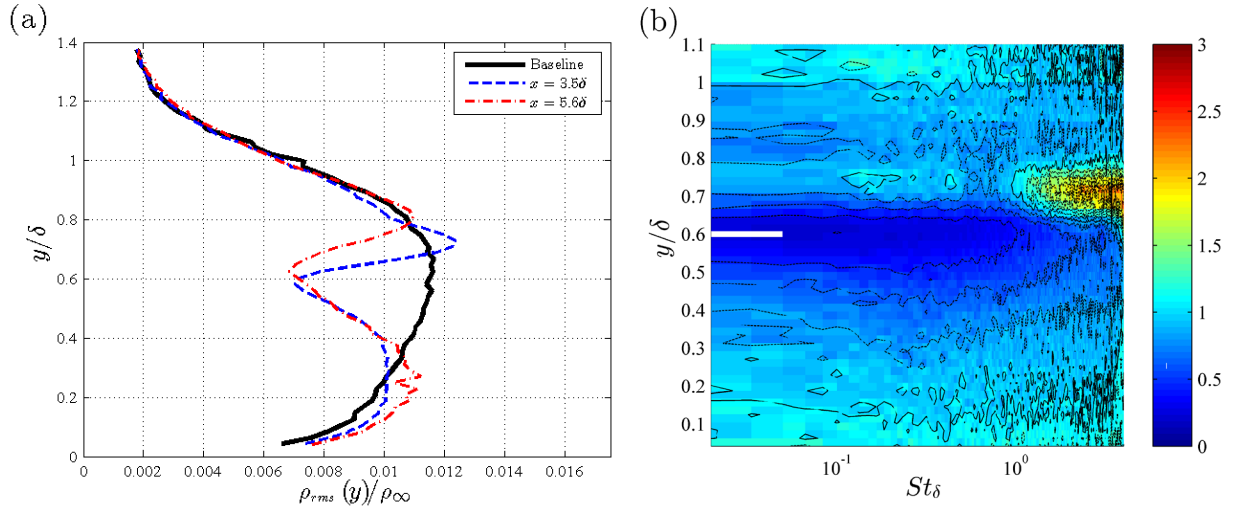

Figure 3. a) $\rho_{rms}(y)/\rho_\infty$ computed from the Strong Reynolds Analogy, and b) contours of baseline-normalized spectrum of $\rho_{rms}(y,St_\delta)/\rho_\infty$ for the $l = 1.6\delta$, $h = 0.6\delta$ single LEBU device. From [12].

Compared to LEBU lengths and heights recommended for drag reduction in turbulent boundary layers, the devices which were found to work best for aero-optic mitigation have a longer streamwise extent, and are placed slightly closer to the wall. Additionally, the aero-optical reduction effect appears immediately downstream of the LEBU device, while it was reported that reductions in local skin friction coefficients typically were not observed for several boundary-layer thicknesses downstream of the device [14, 15]. This suggested that the wake created by the LEBU device affects the large-scale structure directly, while it takes some time and streamwise distance for the modified large-scale structure to affect the small-scale structure near the wall, to reduce the local drag. This result indicated that for aero-optical mitigation, the link between OPD_{rms} and C_f in the canonical boundary layer observed in statistical models of aero-optic distortions [6, 18] is not present in the LEBU-modified boundary layer. This is thought to be a result of the disruption of the global equilibrium state by the LEBU devices through direct modification of the outer-layer structure in the TBL [12].

Mean and fluctuating velocity profiles, $U(y)$ and $u_{rms}(y)$ respectively, measured in the LEBU-modified boundary layer for a select number of cases also provided some insight into the physical mechanism responsible for OPD_{rms} reductions caused by the LEBU devices. It was shown for particularly effective LEBU devices that modification of large-scale structures was in part a result of a decrease in the local mean velocity, which introduces a higher turbulent dissipation without significantly increasing the turbulent velocity fluctuations downstream of the LEBU device [12]. This finding has identified a wider class of passive boundary layer flow control devices, such as thin pin fences and fine screens, should also be investigated with regards to their effect on aero-optic mitigation in the turbulent boundary layer. Several of these devices have already been shown to reduce aero-optical distortions caused by separated shear layers [19] or have been effective at eliminating the local shocks which form over turrets at transonic speeds by slowing the local flow [20].

The aero-optic 'linking equation,' which allows for the estimation of levels of wavefront distortion from statistical measurements of turbulence, was introduced by Sutton in the late 1960s [21]. A simplified form of the equation is often used to estimate levels of optical aberrations;

$$OPD_{rms}^2 = 2K_{GD}^2 \int_0^L \rho_{rms}^2 \Lambda_\rho(y)\, dy, \tag{1}$$

where the root-mean-square density fluctuation profile $\rho_{rms}(y)$ was approximated as proportional to $U(y)u_{rms}(y)$ via the Strong Reynolds Analogy, and $\Lambda_\rho(y)$ is the density correlation length in the wall-normal direction [R5]. In [12], levels of OPD_{rms} were computed from velocity measurements using equation (1) and compared to aero-optically measured OPD_{rms}. The results indicated that aero-optically measured reductions in OPD_{rms} could not be fully accounted for by considering only the modifications to the mean and fluctuating velocity profiles, but that the LEBU device was also modifying turbulent length scales within the boundary layer [12].

While this preliminary work on the effects of LEBU devices on turbulent boundary layers for aero-optic mitigation has been successful in demonstrating significant reductions in OPD_{rms} and identifying some of the physical processes thought to be responsible for these reductions in aero-optical aberrations, several additional experimental objectives were identified for aero-optic LEBU research. These objectives included extending the streamwise extent of study in order to determine how far downstream LEBUs effective for in mitigating aero-optical effects, and investigating the effectiveness of multiple element LEBU devices, including multi-LEBUs and tandem-LEBUs as multi-element LEBUs have been shown to be more effective at reducing large-scale turbulent structures in the TBL [13]. Also, additional wavefront and velocity measurements should be performed in order to better understand the specific mechanism or mechanisms which result in reduced wavefront aberrations downstream of LEBU devices.

In this paper, experimental measurements of aero-optic characterization of LEBU device wake up to 10δ downstream of the LEBU trailing edge are presented for selected single LEBU devices, as well as a number of multi-LEBU and tandem-LEBU devices of different lengths, heights, and streamwise separations. The effectiveness of these LEBU devices on the streamwise extent and overall levels of aero-optic mitigation in the turbulent boundary layer will be assessed. Section II presents the experimental setup and the data reduction procedure. Section III presents analysis and discusses the results of aero-optic wavefront measurements downstream of LEBU devices for a number of different single- and multi-element LEBU configurations. Various wavefront statistics, such as overall levels of aero-optic distortions and wavefront spectra are compared and discussed in detail. Section IV provides conclusions and discusses plans for future work.

II. Experimental Setup

Experimental measurements of the turbulent boundary layer were conducted in the Transonic Wind Tunnel at the University of Notre Dame's Hessert Laboratory for Aerospace Research. The wind tunnel has an open-loop design with a 150:1 inlet contraction ratio, followed by a boundary layer development section, and a boundary layer measurement section. The cross section of the boundary layer development and measurement sections is 9.9 cm by 10.1cm. The total length of the boundary layer development section is variable, and can be lengthened or shortened using 30-cm modular sections to control boundary layer thickness at the measurement section. In the current study, the total length to the optical section is approximately 151 cm. Free-stream velocity was measured using a Pitot probe mounted downstream of the measurement location. For all wavefront measurements, sections of the upper and lower Plexiglass walls were replaced with optical glass windows downstream of the LEBU device to ensure accurate optical characterization of the boundary layer. The boundary layer profile was obtained using a hot-wire anemometer, which is described later, to measure the mean velocity and velocity RMS profiles at a freestream velocity M = 0.4. From these measurements, 99% boundary layer thickness, δ = 2.4 cm, and the displacement thickness, δ^* = 3.15 mm were obtained at the LEBU mounting location.

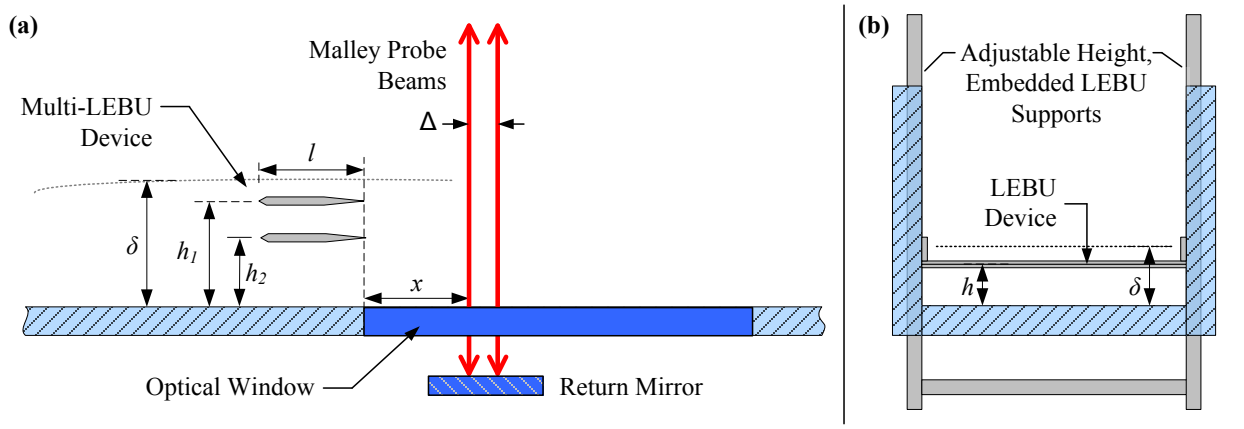

Figure 4. a) Schematic of the experimental setup for Malley probe wavefront and hot-wire velocity measurements downstream of single and multi-LEBU devices, and b) a downstream view of the adjustable-height LEBU mounting mechanism.

To test the effectiveness of LEBU devices, consisting of thin, zero-angle of attack plate or plates, for aero-optic mitigation in the turbulent boundary layer, several LEBU devices with different lengths, manufactured from 0.8 mm thick steel plate, were mounted to the wind tunnel side walls on two vertical sliding supports, as shown in Figure 4, which allowed for the continuous variation of the distance from the wall, *h,* that the LEBU was mounted at. The device spans the width of the test section, and as testing progresses, different LEBU heights (h) and lengths (l) were tested. For multi-LEBU devices, the heights of each element, starting with the outermost and proceeding towards the wall, are denoted as h_1, and h_2 as shown in Figure 1b. For tandem-LEBU devices, the same LEBU length and height were used for both individual LEBUs, and the streamwise spacing is denoted as s, as shown in Figure 1c.

Table 1. Description of tested LEBU devices using Malley probe wavefront sensor.

LEBU Configuration	l/δ	h_1/δ	h_2/δ	s/δ
Single	1.6	0.6	-	-
	1.6	0.5	-	-
Multi	1.6	0.9	0.6	-
	1.6	0.8	0.5	-
	1.6	0.6	0.3	-
Tandem	1.6	0.6	-	4.0
	1.6	0.6	-	8.0

Previous wavefront measurements [9] identified longer single-LEBU devices placed at a height of about 0.5-0.6δ as producing the most significant reduction in OPD_{rms} within 6δ of the LEBU trailing edge. These results were used to choose a select number of single, multi, and tandem LEBU devices to characterize optically up to 10δ. Table 1 contains the descriptions of the LEBU configurations investigated in the present study. For each of these configurations, one dimensional wavefronts were acquired using the two-beam Malley probe wavefront sensor, shown in Figure 5. The operation of the 1-D Malley probe wavefront sensor is described in detail by Gordeyev, et al [6, 22]. Using two beams aligned in the streamwise direction, as shown in Figure 5, each with a diameter of approximately 1 mm, the Malley Probe measures the beam deflection angle $\theta(t)$ for each beam, which is equivalent to the slope of the wavefront in the x-direction of mean flow, $\theta(x,z,t) = d[W(x,z,t)]/dx = d[OPD(x,z,t)]/dx$. Therefore, assuming that the flow is 'frozen' and convecting at some convection velocity U_C as it passes over the aperture, OPD can be computed from time series of deflection angle measurements,

$$OPD(x,z,t) = -U_C \int_0^t \theta(x,z,\tau)\, d\tau \cdot \qquad (2)$$

It follows that OPD_{rms} can be computed from the deflection angle amplitude spectrum using the spectral form of equation 2,

$$OPD_{rms}^2 = 2U_C \int_0^\infty \frac{\left|\hat{\theta}(f)\right|^2}{(2\pi f)^2} df \,. \tag{3}$$

Deflection angle data for each Malley probe measurement were sampled at a rate of 200 kHz for 10 seconds. From this time trace of the deflection angle, a number of quantities including deflection angle amplitude spectrum, one-dimensional wavefronts, and OPD_{rms} can be computed using the frozen-flow assumption, $dx = U_C dt$, where the U_C is computed from the phase delay between readings from two Malley beams aligned in the streamwise direction with separation Δ.

Wavefronts were acquired for an incoming Mach number of $M = 0.4$ at 1 cm intervals for a distance of 24 cm downstream of the trailing edge of each tested LEBU devices, all of which were mounted such that the trailing edge was located at a streamwise location of 148 cm.

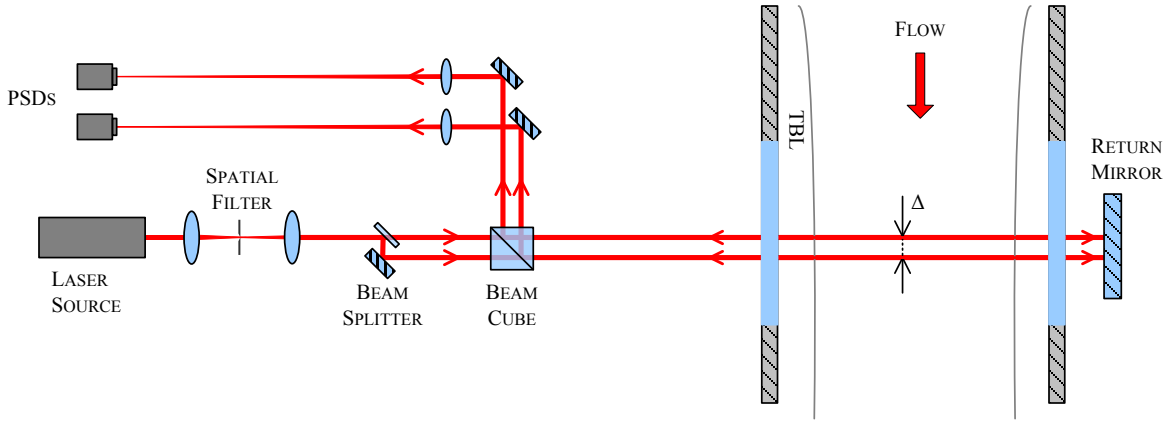

Figure 5. Schematic of the Malley Probe wavefront sensor.

Assuming that the boundary layers on opposite side walls of the wind tunnel test section are statistically independent, the contribution of the LEBU-modified boundary layer, OPD_{rms}^{LEBU} may be isolated from the contribution of the un-modified upper boundary layer using an extension of the statistical relationship shown in [10],

$$OPD_{rms}^{\text{LEBU}} = \sqrt{\left(OPD_{rms}^{\text{DBL}}\right)^2 - \left(OPD_{rms}^{\text{Baseline}}\right)^2 / 2} \,,$$

where OPD_{rms}^{DBL} is the value of OPD_{rms} measured by a wavefront sensor passing through the LEBU-modified boundary layer and the un-modified boundary layer, and $OPD_{rms}^{\text{Baseline}}$ is the value of OPD_{rms} measured by a wavefront sensor passing through two un-modified boundary layers in the control case. Similarly, it is also shown in [10] that deflection angle spectrum of the LEBU-modified boundary layer can be extracted in a similar manner;

$$\hat{\theta}(f)_{\text{LEBU}} = \sqrt{\left(\hat{\theta}(f)_{\text{DBL}}\right)^2 - \left(\hat{\theta}(f)_{\text{Baseline}}\right)^2 / 2} \,. \tag{4}$$

In addition to wavefront measurements, hot-wire velocity profiles were obtained at $x = 6\delta$ downstream of selected LEBU devices. Measurements were obtained using a single hot-wire mounted to a linear traverse and a commercial constant temperature anemometer. Data were sampled at a rate of 200 kHz for 10 seconds at each point in the profile, and the anemometer's built-in low-pass filter was used with a cutoff frequency of 100 kHz. The hot-wire was calibrated in the freestream for Mach numbers ranging from $M = 0.18$ to 0.43. The freestream Mach number for each test was set at $M = 0.4$ to match the freestream velocity of the wavefront measurements.

III. Results & Analysis

A. Single-LEBU Characterization to 10δ

1. Aero-Optic Mitigation Results

Time series of wavefront deflection angle, $\theta(t)$, were measured using the Malley probe for the incoming Mach number 0.4 at a number of locations over a distance of 24 cm downstream of the LEBU devices described in Table 1, as well as for the baseline, no LEBU device, case. Results for both of the single LEBU configurations tested in the

present study show that overall levels of aero-optical distortions were reduced by approximately 20-25% immediately downstream (~1δ) of the devices. Levels of OPD_{rms} in the single LEBU-modified reach a maximum reduction of about 30% in the neighborhood of 4-5δ. As shown in Figure 6, these measurements are in good agreement with previous experiments presented in [12]. Levels of single LEBU modified OPD_{rms} begin to slowly recover towards the baseline levels of OPD_{rms} around streamwise location of 6δ, with the reduction in OPD_{rms} being only 15-20% for single LEBU cases by a distance of 10δ downstream of the LEBU trailing edge.

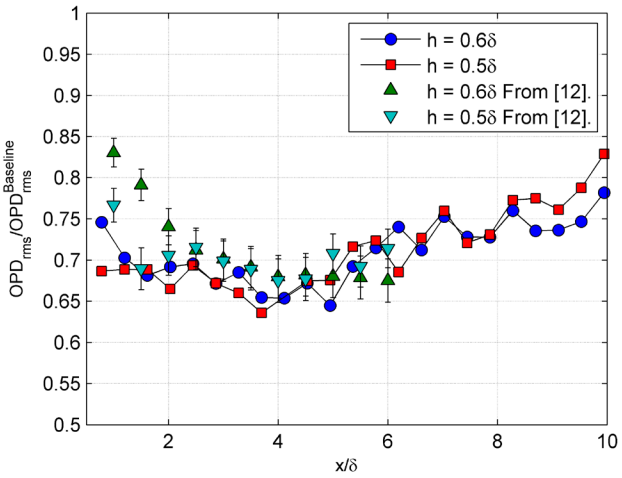

Figure 6. Streamwise development of OPD_{rms} for l/δ = 1.6, h/δ = 0.6, 0.5 compared with results from [12].

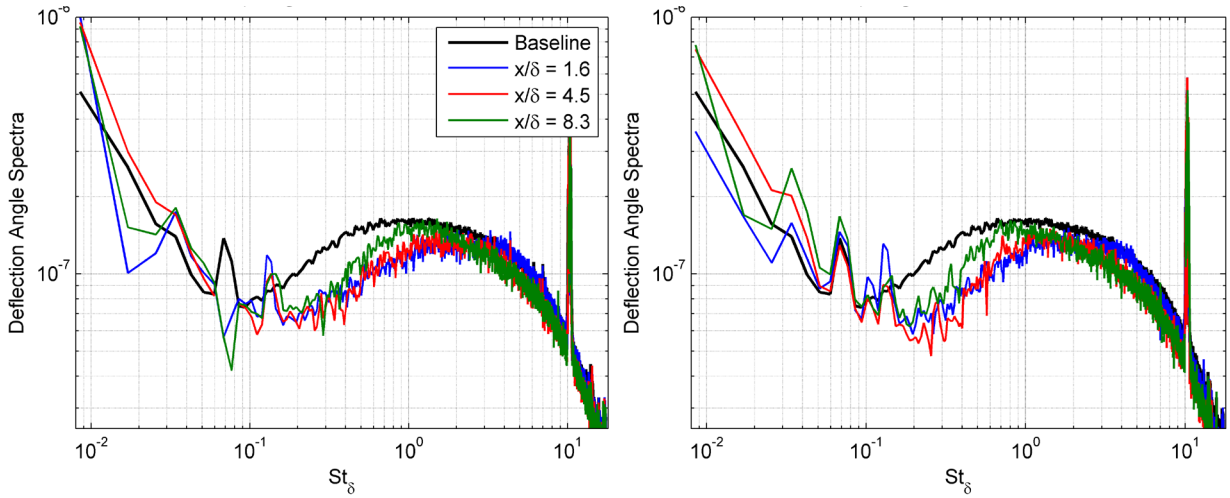

a) Single LEBU, h = 0.6δ **b) Single LEBU, h = 0.5δ**

Figure 7. Malley probe deflection angle spectrum at select streamwise locations for a) h/δ = 0.6, and b) h/δ = 0.5 single LEBU devices.

Single Boundary Layer (SBL) scaled deflection angle spectra were computed using equation (4), and plotted for select streamwise locations in Figure 6 for both h = 0.5δ and h = 0.6δ compared to the baseline TBL deflection angle spectrum. These plots show that just downstream of the LEBU device (x = 1.6δ), there is a significant suppression of large-scale, St_δ < 3, structures, indicating a reduction in size of aero-optically active structures in the TBL. Also shown at 1.6δ is a very slight increase in high-frequency (St_δ > 4) content in the deflection angle spectrum, which likely corresponds to the re-distribution of turbulent kinetic energy to smaller scales by the presence of the LEBU devices. Further downstream at x = 4.5δ, there is a slight increase in the low-frequency region (St_δ ~ 2) with respect to deflection angle spectrum at 1.6δ, although the spectrum in this region is still below the baseline spectrum. In addition, at 4.5δ the increase in spectrum above St_δ > 3 that was shown upstream at 1.6δ has reduced in amplitude below the baseline spectrum. This is most probably a result of the energy cascade, as the reduced energy at low

frequencies has begun to decrease the amount of energy transferred to the high-frequency end of the spectrum, and ultimately reducing the energy content at high-frequency. Further downstream at $x = 8.3\delta$, deflection angle spectrum for both Figure 7a and 7b show that the low-frequency portion of the spectrum in the neighborhood of $St_\delta = 1$ is approaching the baseline deflection angle spectrum value, while both the low and high-frequency portions of the spectrum, $St_\delta < 0.8$ and $St_\delta > 3$ remain below the baseline value.

To better understand the evolution of deflection angle spectrum in the streamwise position as compared to the baseline deflection angle spectrum, the ratio of deflection angle spectrum for LEBU-modified TBLs to baseline TBL spectrum can be defined as

$$C_\theta\left(x/\delta, St_\delta\right) = \frac{\left|\hat{\theta}_{\text{LEBU}}\left(x/\delta, St_\delta\right)\right|}{\left|\hat{\theta}_{\text{Baseline}}\left(x/\delta, St_\delta\right)\right|} - 1, \tag{5}$$

where $C_\theta(x/\delta, St_\delta)$ will be equal to zero where the LEBU-modified spectrum is equal to the baseline spectrum, positive where the LEBU-modified spectrum is increased compared to the baseline, and negative where the LEBU-modified spectrum is less than the baseline spectrum. Contour plots of $C_\theta(x/\delta, St_\delta)$ are presented in Figure 8 for both single LEBU devices. For both cases, Figure 8 shows a significant reduction in large-scale structures below $St_\delta = 3$ that diminishes as distance from the LEBU trailing edge increases. Additionally, a decrease in high-frequency content of the deflection angle spectrum is also shown as the downstream distance increases, which is consistent with the results previously shown in Figure 7.

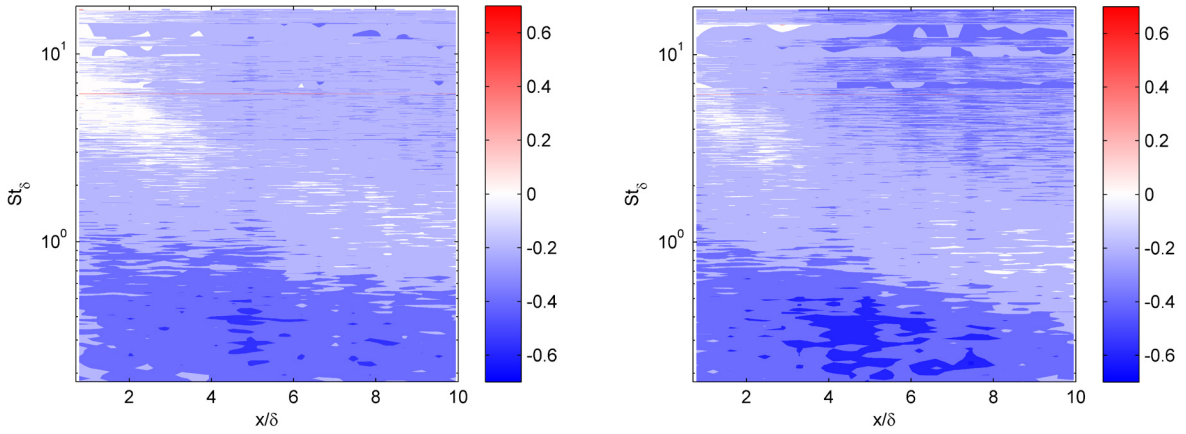

a) Single LEBU, $h = 0.6\delta$ **b) Single LEBU, $h = 0.5\delta$**

Figure 8. Baseline-normalized spectrum surfaces $C_\theta(x/\delta, St_\delta)$ for single LEBU devices of height $h/\delta = 0.6$ (left) and $h/\delta = 0.5$ (right).

One feature that is apparent in the LEBU-modified deflection angle spectrum plotted in Figure 8 that is not evident in Figure 7 is the evolution of the peak of $C_\theta(x/\delta, St_\delta)$ with the downstream distance from the LEBU device, which likely corresponds to the development of the LEBU device wake. The shift of the peak in C_θ to the lower frequencies occurs as the downstream distance increases, eventually approaching a value of $St_\delta = 1$. It has been shown in previous studies of LEBU devices [15-17] that just downstream of the LEBU, there is a momentum-deficit wake that begins at the LEBU trailing edge, and grows with the increasing downstream distance, x, to a point where it is on the order of the TBL thickness δ and interacts with the near-wall layer. If it is assumed that this peak in C_θ corresponds to a coherent structure of some size, γ, then the relationship between the structure size γ and the frequency f_{Peak} at which the maximum in C_θ occurs can be expressed via the frozen flow assumption,

$$\gamma \cong \frac{U_\infty}{f_{Peak}} = \frac{\delta}{St_\delta^{Peak}},$$

where St_δ^{Peak} is the Strouhal number that corresponds to f_{Peak}. If it is assumed that the shift of St_δ^{Peak} toward lower frequencies corresponds to the growth in the size of the LEBU wake, then the half-width, b, of the LEBU wake can be estimated as a function of x from the peak of the normalized spectrum;

$$b(x) \cong \frac{\gamma}{2} = \frac{1}{2}\frac{\delta}{St_\delta^{Peak}}.$$

The result of this estimation for the single LEBU, $h = 0.6\delta$ device is presented in Figure 9 along with measurements of the wake half-width computed from hot-wire velocity profiles obtained in [12]. The comparison shows that the estimate of the wake half-width, b, from the normalized spectrum peaks is in good agreement with direct measurements obtained previously for the same case, and verifies that the evolution of the peak of the normalized spectrum C_θ is a result of the growth of the LEBU wake within the modified TBL.

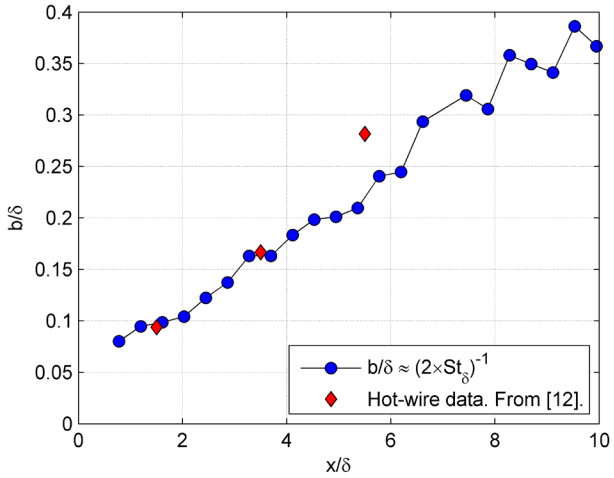

Figure 9. Comparison of wake half-width b estimated from $C_\theta(x/\delta,St_\delta)$ and computed from hot-wire velocity measurements from [12].

Downstream of the location where the LEBU wake reaches the wall, which we will denote as x_w, Lemay, et al. [16] showed that the distribution of the turbulence production and dissipation in the modified TBL recovers to the pre-LEBU boundary layer state. Based on these findings, it is expected that after the LEBU-modified spectrum peak recovers to $St_\delta \approx 1$ (indicating wake-wall interaction), LEBU modified deflection angle spectrum at locations far downstream of x_w will recover to the canonical TBL spectrum. In the present study, it is apparent from the shape of deflection angle spectrum approaching 10δ that the single LEBU-modified TBL is not yet recovered to a canonical state. However, the increase in spectrum in the neighborhood of $St_\delta \sim 1$, coupled with the recovery of OPD_{rms} towards baseline values shown in Figure 6, indicates that the boundary layer is beginning to recover towards the 'baseline' form.

In [12] it was shown from velocity measurements that LEBU mitigation was likely the result of a decrease in the production term on the lower side of the LEBU wake (that is, closer to the wall). This effect has also been observed in other studies [13, 16], although the wake-related drag reduction for LEBU devices was found to be only one part of the full drag reduction mechanism. Savill & Mumford [15] showed that the location of wake-wall interaction downstream of LEBU devices was correlated to the location of the maximum C_f reduction. This location of the maximum C_f reduction was shown to be $>10\delta$ downstream of the device trailing edge for LEBU heights $h > 0.5\delta$ [15]. In [12] and in the present study, maximum reductions in OPD_{rms} have been shown to occur relatively close, within 10δ, to the LEBU trailing edge, and recovery of levels of OPD_{rms} towards baseline values begins to occur upstream of the point at which the wake-wall interaction occurs. These observations are further evidence that the combination of the locally-decreased production and the de-correlation of the inner and outer portions of the TBL resulting from the LEBU wake, as well as the suppression of large-scale coherent structures play an important role in reducing the aero-optic effects of the TBL.

B. Multiple-Element LEBU Devices

While single LEBUs have been shown to give reductions in OPD_{rms} on the order of 30%, the effectiveness of multiple-element LEBU devices, including multi-LEBU (vertically stacked) and tandem LEBU (horizontally spaced) devices, should be assessed to investigate whether or not the additional elements result in any further reduction in levels of OPD_{rms}.

1. Multi LEBU Devices

Malley probe wavefront measurements were obtained in the same manner as described in Section III.A for the multi LEBU devices described in Table 1. From these measurements, overall levels of OPD_{rms} were computed, and

the results are shown, normalized by the baseline OPD_{rms}, in Figure 10. For reference, Figure 10 also shows OPD_{rms} data for the $h = 0.6\delta$ single LEBU case from the previous section.

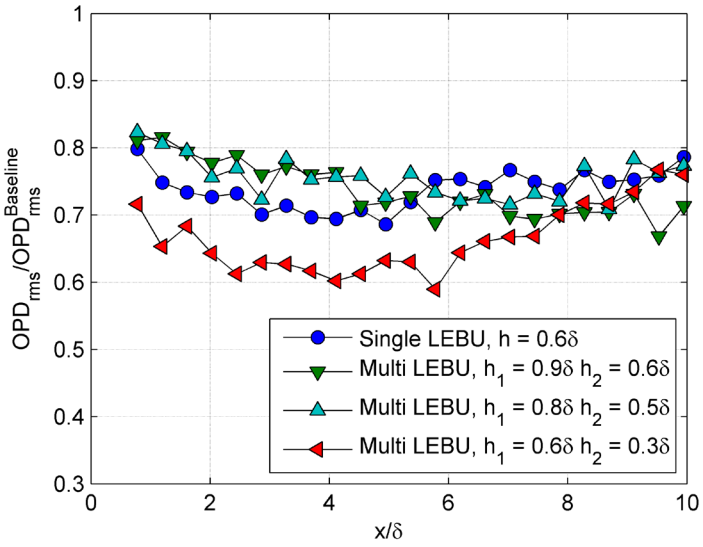

Figure 10. Streamwise development of OPD_{rms} for multi LEBU devices of different heights, compared to h/δ = 0.6 single LEBU results from Section III.A.

For the $h_1/\delta = 0.9$, $h_2/\delta = 0.6$ and $h_1/\delta = 0.8$, $h_2/\delta = 0.5$ multi LEBU configurations, aero-optic distortions were reduced by about 20% immediately downstream of the devices, which compares well with the reductions observed for the single LEBU device with $l/\delta = h/\delta = 0.6$. Further downstream of the LEBU device, the levels of OPD_{rms} for both of these multi LEBU devices continue to decrease with respect to the baseline measurements, reaching a maximum reduction of approximately 30% around the streamwise position of 7δ. Compared to the single LEBU result, this location of the maximum reduction is approximately 2δ further downstream, and is approximately the same strength as the reductions from the single LEBU device. Beyond the location of the maximum reduction for both of these multi LEBUs, the levels of OPD_{rms} for $h_1/\delta = 0.8$, $h_2/\delta = 0.5$ appear to begin recovery towards the un-modified boundary layer state, while OPD_{rms} for $h_1/\delta = 0.9$, $h_2/\delta = 0.6$ is shown to be leveling out around 70% of the baseline value. These results appear to indicate that the effect for multi LEBUs do not seem to be additive, as the results for the $h_1/\delta = 0.9$, $h_2/\delta = 0.6$ multi LEBU do not show a simple increase in the reductions detected for the $h/\delta = 0.6$ single LEBU device.

For the $h_1/\delta = 0.6$, $h_2/\delta = 0.3$ multi LEBU configuration OPD_{rms} was reduced by about 30% immediately downstream of the device trailing edge, and OPD_{rms} continued to decrease, resulted in a large, relatively flat range of reduction between 2δ and 6δ where levels are about 40% less than those of the baseline OPD_{rms}. Beyond 6δ downstream of this multi LEBU device, levels of OPD_{rms} begin to recover toward the un-modified TBL levels, reaching about 80% of the baseline value by 10δ.

Contour plots of $C_\theta(x/\delta, St_\delta)$ are presented in Figure 11 for all three multi LEBU device configurations. For the $h_1/\delta = 0.9$, $h_2/\delta = 0.6$ device, shown in Figure 11a, in the region immediately downstream of the LEBU ($x = 1{-}4\delta$) there is a significant reduction in the deflection angle spectrum over the baseline values below $St_\delta \approx 2$, and an increase above the baseline values in the high-frequency, $St_\delta > 3$, end of the spectrum. This increase over the baseline value is reduced with increasing downstream distance, until after $x \sim 4\delta$, where the high-frequency end of the spectrum ($St_\delta > 2$) is reduced below the baseline values. For the low-frequency portion of the deflection angle amplitude spectrum ($St_\delta < 2$), the strength of the reduction of the multi-LEBU modified spectrum increases, especially around a value of $St_\delta = 0.4$. In addition, as the measurement location increases from 4 to 10δ, the region of low-frequency suppression achieved by this particular LEBU device is reduced slightly in Strouhal number space as the peak of the LEBU-modified deflection angle spectrum approaches the baseline level and baseline location around $St_\delta \approx 1$.

For the $h_1/\delta = 0.8$, $h_2/\delta = 0.5$ device, shown in Figure 11b, the normalized spectrum surface appears qualitatively similar to the results shown in Figure 11a, although quantitatively there are some notable differences. Just downstream of the LEBU trailing edge, a significant decrease in the low-frequency ($St_\delta < 2$) and significant increase in the high-frequency ($St_\delta > 2$) ranges of the deflection angle spectrum are observed with respect to the baseline

spectrum. However, the strength (or amount of increase) of the high-frequency portion of the spectrum appears to be reduced slightly in comparison to the $h_1/\delta = 0.9$, $h_2/\delta = 0.6$ device. Furthermore, the streamwise extent of this region of high-frequency increase is limited to about 3δ. The reduction in the low-frequency range of the spectrum appears to be rather similar in strength and size in Strouhal number space, with the only major difference being that a portion of the deflection angle spectrum for the $h_1/\delta = 0.8$, $h_2/\delta = 0.5$ device in the neighborhood of $St_\delta \approx 2$ remains at the level of the baseline amplitude spectrum, and shifts to a St_δ of nearly 1 as the measurement station approaches 10δ.

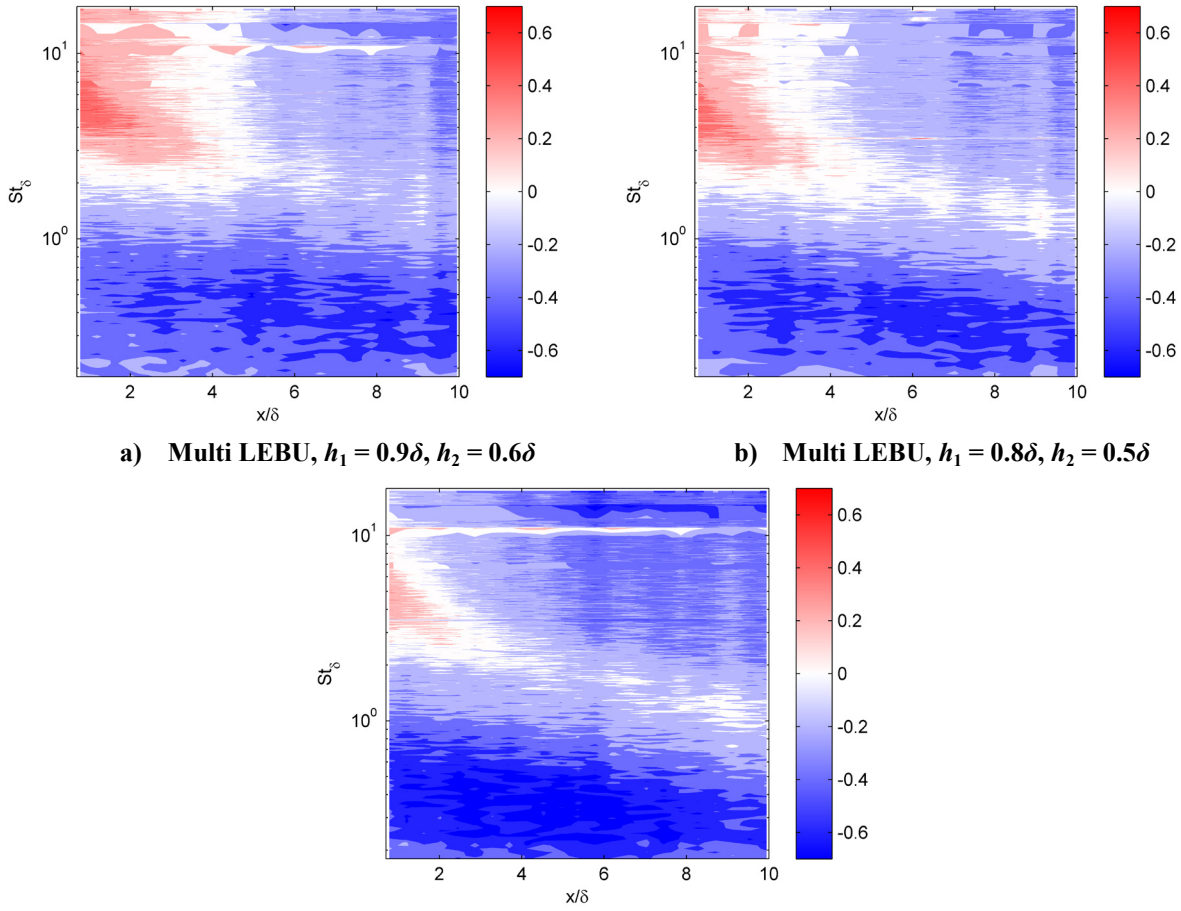

a) Multi LEBU, $h_1 = 0.9\delta$, $h_2 = 0.6\delta$ **b) Multi LEBU, $h_1 = 0.8\delta$, $h_2 = 0.5\delta$**

c) Multi LEBU, $h_1 = 0.6\delta$, $h_2 = 0.3\delta$

Figure 11. Baseline-normalized spectrum surfaces $C_\theta(x/\delta, St_\delta)$ for multi LEBU devices.

The normalized spectrum surface, shown in Figure 11c, for the $h_1/\delta = 0.6$, $h_2/\delta = 0.3$ multi LEBU device bears some qualitative similarities to the spectrum shown in Figure 11a and Figure 11b, respectively, but quantitatively the effect of this LEBU is shown to be much more significant than the previous two cases. Immediately downstream of the LEBU trailing edge, the LEBU modified deflection angle spectrum is reduced by approximately 60% compared to the baseline deflection angle spectrum below $St_\delta = 2$. This strong low-frequency reduction is sustained up to approximately 6δ, where the low-frequency ($St_\delta < 2$) end of the deflection angle spectrum begins to recover towards the baseline spectrum. Also just downstream of the LEBU device, there is a slight 20% increase in a portion of the high-frequency ($2-7\delta$) end of the deflection angle spectrum. This increase disappears entirely beyond 3δ downstream of the LEBU device. Beyond $3\text{-}4\delta$, the entire high-frequency range of the deflection angle spectrum shows a reduction over the baseline of approximately 40% above $St_\delta = 3$, indicating a decrease in dissipation relative to the baseline flow. This effect is likely the result of the suppression of low-frequency ($St_\delta < 2$) structures beginning immediately downstream of the LEBU trailing edge which yields an overall reduction in the amount of energy cascading into small scales. At $x = 10\delta$, the peak of the LEBU modified spectrum is approaching $St_\delta = 1$, which is another indication (along with the recovery of overall levels of OPD_{rms} towards the baseline value) that the aero-optic reduction effects of this LEBU configuration are starting to wear off by 10δ.

2. Tandem -LEBU Devices

Malley probe wavefront measurements were also performed for the tandem LEBU devices described in Table 1. Overall levels of OPD_{rms} for each tandem LEBU device were computed for streamwise locations $x = 0.8\delta$ to 10δ, and the results, normalized by the baseline OPD_{rms}, are shown in Figure 12. As a reference, Figure 12 also shows OPD_{rms} data for the $h = 0.6\delta$ single LEBU and $h_1 = 0.6\delta$, $h_2 = 0.3\delta$ multi LEBU from the previous sections. For both tandem LEBU configurations, the level of aero-optic distortions just downstream of the LEBU is reduced by approximately 30%. Further downstream, levels of OPD_{rms} for the $s = 4\delta$ tandem LEBU device remain relatively constant around 70% of the baseline value until $x \approx 10\delta$. Downstream of it, the aero-optical distortions appear to be increasing slightly towards the baseline value. For the $s = 8\delta$ tandem LEBU device, OPD_{rms} continues to decrease further downstream until reaching a region of maximum reduction between $4-6\delta$, where the levels of LEBU-modified OPD_{rms} are reduced by about 42% compared to the baseline. Downstream of the streamwise location of 6δ, the levels of OPD_{rms} begin to recover slightly towards the baseline levels, but the rate of recovery is more gradual than what was observed for the $h_1 = 0.6\delta$, $h_2 = 0.3\delta$ multi LEBU device (which had the largest maximum reduction in OPD_{rms}), with the OPD_{rms} at 9-10δ being approximately 35% lower than the baseline measurement. This result indicates that the tandem LEBU device results in the most significant reduction in OPD_{rms} over a longer streamwise extent than any of the other tested LEBU configurations.

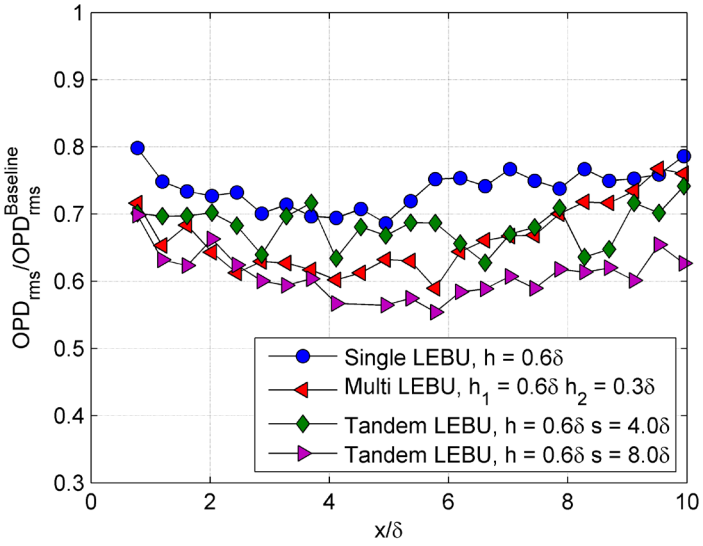

Figure 12. Streamwise development of OPD_{rms} for Tandem LEBU devices with separations $s = 4\ \delta$ and 8δ, compared to the best-performing single and multi-LEBU results.

A streamwise evolution of the baseline-normalized deflection angle spectra are presented in Figure 13 for the $s = 4\delta$ and 8δ tandem LEBU devices. Results in Figure 13a show that for $s = 4\delta$ LEBU device, the deflection angle spectrum is increased by about 20% over the baseline spectrum immediately downstream of the LEBU wake above $St_\delta = 10$. This increase persists in the deflection angle spectrum until the streamwise location of approximately 8δ downstream. Just downstream of this tandem LEBU device, there is a significant decrease of the LEBU modified spectrum compared to the baseline below $St_\delta = 3$, particularly in the low-frequency end of the spectrum corresponding to $St\delta < 1$. By $x = 3\delta$, the region of reduction in the deflection angle spectrum expands such that the spectrum is reduced in the range $St_\delta < 8$. This effect remains mostly the same over the streamwise extent of the study, with the exception of the shift in the location of the local maximum in the normalized deflection angle spectrum from $St_\delta \approx 5$ just downstream of the LEBU to $St_\delta \approx 1.5$ around $x = 10\delta$. This feature of the spectrum likely corresponds to the spanwise growth of the LEBU wake within the TBL as it moves downstream. Additionally, approaching 10δ, there is an increased suppression of the LEBU-modified spectrum in the region, $St_\delta > 2$, which is likely the result of the suppression of large-scale structures further upstream, similar to single LEBU devices.

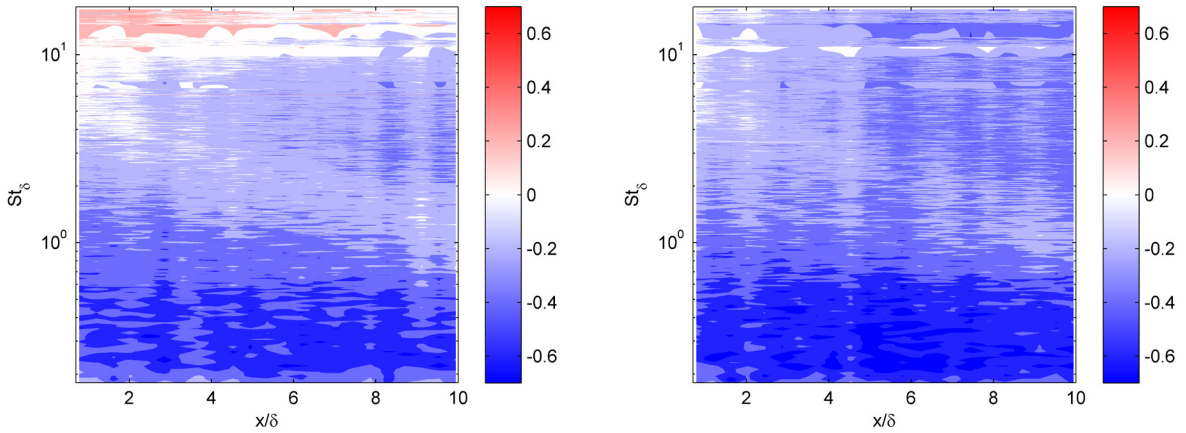

a) Tandem LEBU, $h = 0.6\delta$, $s = 4\delta$ **b) Tandem LEBU, $h = 0.6\delta$, $s = 8\delta$**

Figure 13. Baseline-normalized spectrum surfaces $C_\theta(x/\delta, St_\delta)$ for a) $s = 4\ \delta$ and b) $s = 8\delta$ tandem LEBU devices.

Normalized deflection angle results for the $s = 8\delta$ tandem LEBU, shown in Figure 13b, do not show, unlike the 4δ tandem LEBU, any increase in the spectrum amplitude with respect to the baseline spectrum,. For the $s = 8\delta$ tandem LEBU device, the region of suppression in the low-frequency end of the spectrum ($St_\delta < 1$) shows an overall stronger suppression of aero-optic spectrum compared to the 4δ tandem LEBU at the same frequency range. Additionally, for streamwise locations $x > 4\delta$ there is an increasingly strong reduction in the high-frequency end of the deflection angle spectrum. This is likely is a result a reduction in the amount of energy cascading into smaller-scales at which turbulence dissipation occurs. For this tandem LEBU, the baseline-normalized spectrum peak is also observed to shift to lower-frequencies as the streamwise location increases, moving from a value around $St_\delta = 6$ to about $St_\delta = 1$. At 10δ, however, the suppression of large-scale structures ($St_\delta < 1$) is still rather strong, so it is possible that levels of optical aberrations will remain low for several more TBL thicknesses before beginning to relax to the baseline values.

C. Streamwise Wavefront Correlation Length

As in [12], streamwise wavefront correlation functions of Malley probe wavefront data were computed by taking the inverse Fourier transform of the single-boundary layer wavefront power spectra, $\left|\hat{\theta}(f)\right|^2$ to obtain the autocorrelation in time at each streamwise measurement location, $R(\tau) = \mathrm{F}^{-1}\left\{\left|\hat{W}(f)\right|^2\right\}$, where Φ^{-1} denotes the inverse Fourier transform. The frozen-flow approximation, $\Delta x = U_C\tau$, was then applied to estimate the streamwise wavefront correlation function, $R(\Delta x)$. The streamwise correlation lengths, Λ_x, defined as the Δx location of the first zero crossing, were computed from $R(\Delta x)$ at each streamwise location. Figure 14 presents Λ_x computed for the single, multi, and tandem LEBUs that gave the largest reduction in OPD_{rms} from the previous sections. The data are normalized by the baseline correlation length computed from the model correlation curve presented in [23] for large-aperture wavefront measurements, which was shown in [12] to be in good agreement with experimental measurements of the streamwise correlation function of the un-modified turbulent boundary layer. The largest reduction of wavefront correlation length Λ_x is given by the multi-LEBU device just downstream ($x < 2\delta$) of the LEBU trailing edge. As the streamwise distance increases beyond 3δ, however, the correlation length for multi LEBU wavefronts increases above those measured for the single and tandem LEBUs. Comparing the single and tandem LEBU correlation length results, the streamwise development of Λ_x is very similar, with the values of Λ_x for the tandem LEBU being slightly less than those of the single LEBU device. These results show that for all three LEBU devices, the maximum reduction in the streamwise correlation length occurs close to the LEBU trailing edge, within 1-3δ. For streamwise locations $x > 3\delta$ downstream, there is a gradual increase in the Λ_x towards the baseline value, with the multi-LEBU device reaching the baseline value by about 10δ. The single and tandem LEBU correlation lengths recover to about 0.85 of the baseline by 10δ. At the streamwise location of $x = 6\delta$, which is

where velocity measurements were obtained, the single, multi, and tandem LEBU correlation lengths were found to be about $0.80\,\Lambda_x^{Baseline}$, $0.86\,\Lambda_x^{Baseline}$, and $0.75\,\Lambda_x^{Baseline}$, respectively.

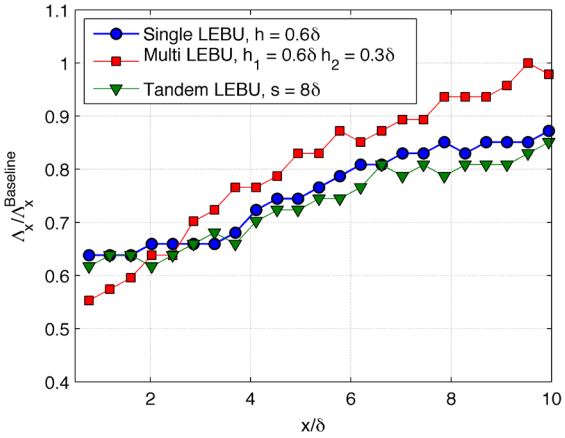

Figure 14. Wavefront correlation lengths as a function of downstream distance.

D. Hot-Wire Velocity Measurements at $x = 6\delta$

To further understand the relationship between the effect of multi-element LEBUs on aero-optic distortions in turbulent boundary layers and their effect on the boundary layer flow, hot-wire velocity profiles were measured at the streamwise location $x = 6\delta$ for the $h/\delta = 0.6$, 0.3 multi LEBU and $s = 8\delta$ tandem LEBU devices. This streamwise location was chosen because it was approximately where both configurations showed the largest reductions in OPD_{rms}. Mean and RMS velocity profiles, normalized by the freestream velocity, are shown in Figure 15. The wall-normal coordinate y is normalized by the boundary layer thickness, δ.

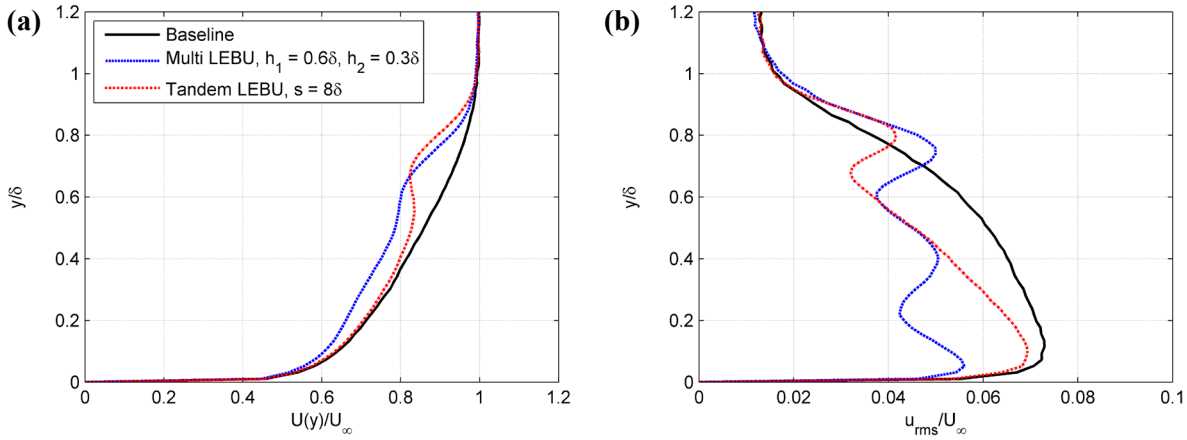

Figure 15. (a) Mean and (b) root-mean-square velocity profiles for multiple-element LEBU devices at $x = 6\delta$.

In the mean velocity profiles, Figure 15a, a region of wake-deficit was observed for the tandem LEBU device which encompassed the range from approximately 0.4δ to 0.9δ in the wall-normal direction. The general shape of the tandem LEBU velocity deficit is consistent with results for the single-LEBU velocity profiles from [12]. For the multi LEBU configuration however, the range of the velocity deficit is much larger in the spanwise direction, with significant reductions in mean velocity from $y = 0.1\delta$ to about 0.9δ. For both multi-element LEBUs, the mean flow characteristics above and below the wake-deficit regions do not appear to be significantly modified. In Figure 16b, the profiles of the root-mean-square of the fluctuating velocity component, u_{rms}, are presented. For both multi-element LEBU devices, there is a significant reduction of velocity fluctuations inside the wake, and the reductions in fluctuating velocity are shown to extend closer to the wall for both LEBUs presented than the effect of the LEBU wake on the mean velocity profiles. Above the location of the LEBU devices in the fluctuating velocity profiles, there is a small peak in fluctuating velocity on the uppermost side of the mean-velocity wake region, with the peak being stronger and wider for the multi LEBU device. In [12], it was discussed that one possible explanation for this

localized increase in fluctuating velocity is that the local velocity gradient, dU/dy, above the LEBU device is increased by the LEBU wake. This increase in dU/dy then results in an increase in the turbulent fluctuating velocity component downstream of the LEBU device, as the dominant turbulence production term, $u'v'(dU/dy)$, is proportional to the mean velocity gradient. This explanation is consistent with the findings of previous investigations of LEBU-modified turbulent boundary layers [13,16].

In [6, 22] it was shown that using by the Strong Reynolds Analogy, the instantaneous density fluctuations in the turbulent boundary layer for an adiabatic wall are proportional to the product of the mean velocity U and fluctuating velocity u' components, $\rho(y,t) \sim U(y)u'(y,t)$. Therefore, the root-mean-square of the density fluctuations is given as

$$\frac{\rho_{rms}(y)}{\rho_\infty} \approx r(\gamma-1)M_\infty^2 \frac{U(y)u_{rms}(y)}{U_\infty^2}, \tag{6}$$

where ρ_{rms} is the root-mean-square density fluctuations, ρ_∞ is the freestream density, r is the recovery factor, and γ is the specific heat ratio. Substituting equation (6) into the Sutton's linking equation (1), it can be shown that levels of optical aberrations can be predicted from the velocity field as follows [9]

$$OPD_{rms} = \sqrt{2}K_{GD}\rho_\infty \delta M_\infty^2(\gamma-1)\left[\int_0^\infty r^2 \left(\frac{U(y)u_{rms}(y)}{U_\infty^2}\right)^2 \frac{\Lambda_\rho(y)}{\delta} d\left(\frac{y}{\delta}\right)\right]^{1/2}. \tag{7}$$

From the relationship shown in (6) between velocity statistics and density fluctuations in the turbulent boundary layer, the power spectral density of the instantaneous density fluctuations, $\rho(y,t) \sim U(y)u'(y,t)$, can be estimated as $S_{SRA}(y,f) = \mathbf{F}\left\{\left[U(y)u'(y,t)\right]^2\right\}$, where $\mathbf{\Phi}$ denotes the Fourier transform. To identify where LEBU devices are causing reductions in OPD_{rms} in both frequency and wall-normal space, the ratio of power spectra of the LEBU-modified boundary layer to the power spectra of the baseline power spectra,

$$C_{SRA}(y/\delta, St_\delta) = \frac{S_{SRA}^{LEBU}(y/\delta, St_\delta)}{S_{SRA}^{Baseline}(y/\delta, St_\delta)}, \tag{8}$$

was computed in the same manner as in [12]. Filled contour plots of this ratio are shown in Figure 16. Note that values $C_{SRA} < 1$ indicate a reduction in the product $U(y)u_{rms}(y)$ for the LEBU-modified TBL. Similarly, values of $C_{SRA} > 1$ correspond to a location of increase in LEBU-modified S_{SRA} in comparison to the baseline measurement. Additionally, the vertical lines of $C_{SRA}(y/\delta, St_\delta) < 0.5$ near $St_\delta = 3$ and $St_\delta = 4$ correspond to electronic interference present in the hot-wire anemometer data.

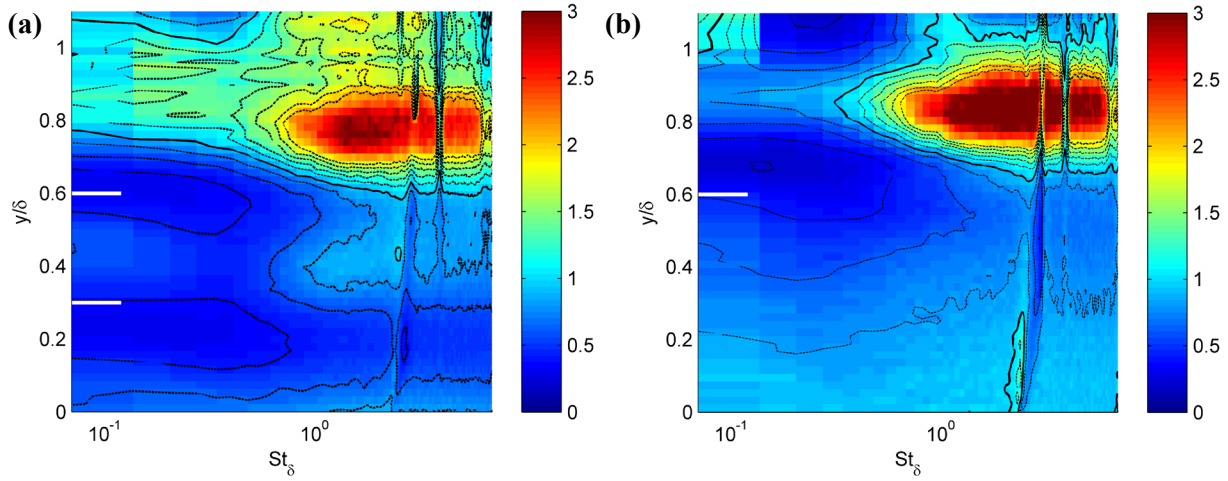

Figure 16. Contour plot of $C_{SRA}(y/\delta,St_\delta)$ at $x = 6\delta$ for (a) $h_1 = 0.6\delta$, $h_2 = 0.3\delta$ multi LEBU and (b) $s = 8\delta$ tandem LEBU devices. LEBU element height is marked by white lines, and the solid black contour indicates where $C_{SRA}(y/\delta,St_\delta) = 1.0$.

Figure 16a shows $C_{SRA}(y/\delta,St_\delta)$ for the $h_1 = 0.6\delta$, $h_2 = 0.3\delta$ multi LEBU device, and Figure 16b shows $C_{SRA}(y/\delta,St_\delta)$ for the $s = 8\delta$ tandem LEBU device. For the multi LEBU configuration in Figure 16a, a large region of

suppression of spectra below St_δ = 1 is observed over the span 0 < y/δ < 0.8. Above St_δ = 1, there is also a suppression in spectra for y/δ < 0.3 for the multi LEBU. In the span between the LEBU elements, 0.3 < y/δ < 0.6, approximately no increase or decrease in spectra above St_δ = 1 with respect to baseline levels. Above y/δ = 0.6, there is a significant increase in spectra above St_δ = 0.5. For s = 8δ tandem LEBU case shown in Figure 16b, C_{SRA} is significantly reduced over the range 0.2 < y/δ < 0.9 for St_δ < 1. Below y/δ = 0.2, the tandem LEBU spectra is reduced by about 20% compared to baseline spectra over the full range of St_δ. Above y/δ = 0.7 there is a significant increase in C_{SRA} in the high-frequency, St_δ > 1, region. It [12], it was indicated that the significant increase in C_{SRA} above the LEBU device likely corresponds to the 'spike' in u_{rms} above the LEBU which is a result of increased production of small-scale turbulent structures on the upper side of the LEBU wake [16]. These results for the multi and tandem LEBUs are consistent with the spectral results obtained for single LEBU devices in [12] (Figure 3b), although the spanwise extent of the regions of low-frequency suppression of C_{SRA} is larger than that observed for single LEBUs, extending all the way to the wall.

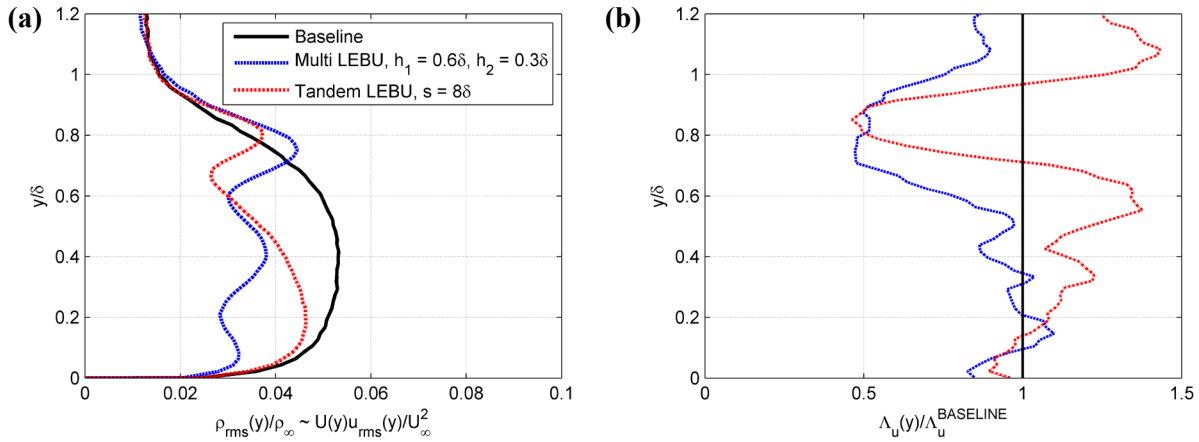

Figure 17. (a) Freestream normalized product of mean and fluctuating velocities for multiple-element LEBU devices at streamwise location x = 6δ, and (b) baseline normalized streamwise velocity correlation length profiles $\Lambda_u(y)$.

The wall-normal profiles of the term $U(y)u_{rms}(y)$, which is proportional to the ρ_{rms}(y), can be computed either directly from velocity time series or by integrating the power spectra $S_{SRA}(y,f)$ in the frequency domain; $U(y)u_{rms}(y) = \left(\int_0^\infty S_{SRA}(y,f)\,df\right)^{1/2}$. Profiles of this product, normalized by the square of the freestream velocity, are presented in Figure 17a at the streamwise location x = 6δ for the multi and tandem LEBU cases from Figure 16. These profiles show a reduction in the wake downstream of both of the LEBU devices with respect to the baseline profile, which indicates a reduction in the density fluctuations in this region. However, using the measured profiles and the density correlation length for the *canonical* boundary layer, $\Lambda_y(y)$, equation (7) predicts that levels of OPD_{rms} are only reduced by about 25% and 17% for the multi and tandem LEBU device, respectively. These predictions are both less than the experimentally measured reductions of 35% for the multi-LEBU and 41% for the tandem LEBU at the same streamwise location. It was shown in Figure 15 that in the LEBU wake, there is a reduction in streamwise wavefront correlation length, Λ_x, between 14-35%, depending on the LEBU device, at x/δ = 6. If it is assumed that $\Lambda_y(y)$ for the LEBU modified boundary layer is proportional to Λ_x, equation (7) now predicts a reduction in OPD_{rms} of approximately 30% for the multi LEBU, and 28% for the tandem LEBU; both of these results still under-predict the reduction in OPD_{rms}, although they are better estimates than using the canonical TBL density correlation length. One potential reason for this under-prediction is that Λ_x is a correlation of turbulent fluctuations integrated through the boundary layer, while the correlation function in equation (7), $\Lambda_\rho(y)$, is not a constant, but a function of wall-normal distance, y. As a result of this functional dependence, wall-normal variations in the actual correlation function induced by the LEBU devices could affect the integrand of equation (7) differently than simply approximating the correlation length as the canonical correlation function scaled by Λ_x. To investigate this, the streamwise autocorrelation $R_u(\tau, y)$ of fluctuating velocity, $u'(t, y)$, was computed for each y-location, and converted to streamwise velocity correlation lengths by the frozen flow approximation, this time using the local mean velocity; $\Delta x = U(y)\tau$. Profiles of the streamwise velocity correlation length, $\Lambda_u(y)$, were computed by integrating $R_u(\Delta x, y)$ to the first zero crossing. The results for the h_1 = 0.6δ, h_2 = 0.3δ multi LEBU and s = 8δ tandem

LEBU are plotted in Figure 17b, normalized by the baseline correlation length profile. Using the velocity correlation profiles from Figure 17b in equation (7) to compute levels of OPD_{rms} for the multi and tandem LEBUs showed reductions of 34% and 18%, respectively. The estimate of OPD_{rms} from equation (7) using $\Lambda_u(y)$ to approximate the density correlation length the multi LEBU device is in good agreement with the level of OPD_{rms} measured with the Malley probe. However, the estimate of OPD_{rms} for the tandem LEBU using $\Lambda_u(y)$ is not in good agreement with Malley probe measured levels of OPD_{rms}, underestimating levels of OPD_{rms} by 23%. One possible explanation for why $\Lambda_u(y)$ is a poor estimate of $\Lambda_\rho(y)$ for the tandem LEBU is that the wake of the far upstream LEBU element (which is about 15δ upstream of the measurement location) interacts and combines with the wake of the downstream LEBU element [15]. The presence of the more developed wake of the upstream LEBU element, strengthened by the wake of the nearer LEBU element, may contribute to the increase in streamwise correlation length shown in Figure 17b for the tandem LEBU device.

IV. Conclusions & Future Work

This paper has presented results from an experimental investigation of compressible, turbulent boundary layer flow control using single-element and multiple-element Large-Eddy Breakup devices for the purpose of aero-optic mitigation. One-dimensional wavefront measurements of OPD_{rms} in the region up to 10δ downstream of the LEBU devices of different single-element and multiple-element configurations demonstrated that an optimal LEBU configuration for aero-optic mitigation is two-element tandem LEBU with $l = 1.6\delta$, $h = 0.6\delta$, and $s = 8\delta$. This configuration gave the maximum reduction in OPD_{rms} of more than 40% downstream of the device to about 5δ, compared to the baseline measurements, and reductions greater than about 35% over a large streamwise range between 1δ and 10δ. Similar reductions in OPD_{rms} of 35% were also shown for a multi-LEBU device with $l = 1.6\delta$, $h_1 = 0.6\delta$, $h_2 = 0.3\delta$, although the streamwise extent of the reduction was limited to about 4δ, after which levels of OPD_{rms} appeared be rapidly recovering towards the baseline state. Levels of aero-optic mitigation for two tested multi-element LEBU configurations were shown to be better than levels of mitigation achieved by single-element LEBU devices alone.

In comparison to multi-element LEBUs identified as optimal for drag reduction in turbulent boundary layers, the results of this study are in agreement with previous studies where tandem-LEBU configurations with elements' spacing on the order of 5-10δ were found to be optimal [15,17], although the device length used in this study is slightly longer, and the height is smaller than those used for the drag reduction studies [17]. Previously-collected comparisons between velocity-based predictions of OPD_{rms} from equation (1) and one-dimensional wavefront measurements of OPD_{rms} [12] indicated that the reduced turbulence production term on the lower side of the LEBU wake was an important factor in reducing levels of aero-optic distortions; also a reduction in wall-normal velocity correlation was found to be another significant contribution to reducing aero-optical distortions.

From the baseline-normalized Malley probe spectrum, estimations of the streamwise evolution of the LEBU wake within the modified TBL were shown to be consistent with previous, hot-wire-based, experimental measurements [12], and provided further indirect evidence that the relationship between levels of OPD_{rms} and C_f found in canonical turbulent boundary layers is not valid in manipulated boundary layers. The location of maximum reduction in OPD_{rms} was shown to occur significantly closer to the LEBU trailing edge than the locations at which previous researchers have shown the minimum C_f occurs [15].

As a result of these findings, it was suggested that additional classes of passive manipulators, including screens and pin-fences, may be effective at mitigating aero-optic effects of TBLs due to their ability to break up large-scale turbulent structures and re-distribute energy into smaller (and therefore, less-optically-active) dissipative scales. The greater effectiveness of tandem LEBU devices in comparison to multi LEBU devices, which were born out of fine screens and honeycombs [13], raises some interesting questions about whether or not these types of passive manipulators would be effective on their own over large distances downstream of the flow manipulator, or whether their effectiveness could be extended through the use of a combination of LEBU-type and screen-type TBL manipulators.

Previous parametric investigations of the optimal LEBU device length $l = 1.6\delta$ LEBUs provided the largest reductions in OPD_{rms} for single LEBU configurations. However, these length devices were the longest in the parametric investigation, and it is possible that even longer LEBUs could produce additional aero-optic mitigation. The effectiveness of tandem LEBU devices gives some indication that this is possible. Future work will include aero-optic characterizations of very long, $l = 4$-10δ, LEBU devices, to see if extremely long manipulator lengths will give any additional suppression of TBL aero-optic distortions. Additional hot-wire velocity characterization of the LEBU wake up to 10δ for selected LEBU cases identified as effective in this paper and in [12] will also be performed. Results from these measurements will be used to investigate the relationship between OPD_{rms} computed

via equation (1) in the LEBU-modified TBL and directly measured levels of OPD_{rms}, and the relationship between the streamwise correlation functions of point-velocity measurements and aero-optic wavefront measurements.

Acknowledgments

This work is supported by the Air Force Office of Scientific Research, Grant number FA9550-12-1-0060. The U.S. Government is authorized to reproduce and distribute reprints for governmental purposes notwithstanding any copyright notation thereon.

References

[1] Gladstone, J.H., and Dale, T.P., "Researches on the Refraction, Dispersion, and Sensitiveness of Liquids," *Philosophical Transactions of the Royal Society of London,* **153**, pp. 317-343, 1863.

[2] Gardner, W. J., Hidaka, Y., and Tanzawa, T., "Refractivity of Combustion Gases," *Combust. and Flame ,* **40**, pp. 213-219, 1980.

[3] Jumper, E.J., and Fitzgerald, E.J., 2001, "Recent Advances in Aero-Optics," *Progress in Aerospace Sciences,* 37, 299-339.

[4] Wang, M., Mani, A., and Gordeyev, S., "Physics and Computation of Aero-Optics", *Annual Review of Fluid Mechanics*, Vol. 44, pp. 299-321, 2012.

[5] Gordeyev, S., Cress, J., and Jumper, E., "Far-Field Laser Intensity Drop-Outs Caused by Turbulent Boundary Layers", *Journal of Directed Energy*, 5(1), pp. 58-75, Spring 2013.

[6] Gordeyev, S., Smith, A.E., Cress, J.A., and Jumper, E.J., "Experimental studies of aero-optical properties of subsonic turbulent boundary layers," accepted for publication in *Journal of Fluid Mechanics*, 2013.

[7] Wang, K. and Wang, M., "Aero-optics of subsonic turbulent boundary layers," *Journal of Fluid Mechanics*, Vol. 696, pp. 122-151, 2012.

[8] White, M.D., and Visbal, M.R., "Simulation of Aero-Optical interactions in Transonic Boundary Layers," 42nd AIAA Plasmadynamics and Lasers Conference, 27-30 June 2011, Honolulu, Hawaii, AIAA-2011-3279.

[9] Cress, J., *Optical Aberrations Cause by Coherent Structures in a Subsonic, Compressible, Turbulent Boundary Layer,* PhD thesis, University of Notre Dame, 2010.

[10] J. Cress, S. Gordeyev and E. Jumper "Aero-Optical Measurements in a Heated, Subsonic, Turbulent Boundary Layer" , 48th Aerospace Science Meeting and Exhibit, Orlando, Florida, 4-7 Jan, 2010, AIAA Paper 2010-0434.

[11] Smith, A.E., and Gordeyev, S. "The Effects of Wall Cooling on Aero-Optical Aberrations Caused by Subsonic Turbulent Boundary Layers," 44th AIAA Plasmadynamics and Lasers Conference, 24-27 June 2013, San Diego, California, AIAA Paper 2013-3133.

[12] Smith, A.E., and Gordeyev, S., "Evaluation of Passive Boundary Layer Flow Control Methods for Aero-Optic Mitigation," 51st AIAA Aerospace Sciences Meeting, 6-10 Jan 2013, Grapevine, TX, AIAA Paper 2013-0718.

[13] Corke, T.C., *A New View on Origin, Role, and Manipulation of Large Scales in Turbulent Boundary Layers*, Ph.D. Thesis, Illinois Inst. of Technology, Chicago, IL, Dec. 1981.

[14] Hefner, J.N., Weinstein, L.M., and Bushnell, D.M., "Large-Eddy Breakup Scheme for Turbulent Viscous Drag Reduction," *Proc. Viscous Drag Reduction Symp., Dallas. AIAA Prog. Astro. Aero.* 72*,* 110-127. (1979)

[15] Savill, A.M., and Mumford, J.C., "Manipulation of turbulent boundary layers by outer-layer devices: skin-friction and flow-visualization results," *J. Fluid Mech.*, 191, 389-418, 1988.

[16] Lemay, J., Delville, J., and Bonnet, J., "Turbulent kinetic energy balance in a LEBU modified turbulent boundary layer," *Experiments in Fluids*, **9**(6), 301-308, 1990.

[17] Anders, J.B., "Outer-Layer Manipulators for Turbulent Drag Reduction." In D.M. Bushnell and J.N. Hefner (Eds.), *Viscous Drag Reduction in Boundary Layers*, (pp. 263-284), Washington, DC: AIAA, 1990.

[18] Wyckham, C., and Smits, A., "Aero-Optic Distortion in Transonic and Hypersonic Turbulent Boundary Layers," *AIAA Journal*, Vol. 47, No. 9, pp. 2158-2168, 2009.

[19] Gordeyev, S., Cress, J., Smith, A.E., and Jumper, E., **"**Improvement in Optical Environment over Turrets with Flat Window Using Passive Flow Control,**"** *41th AIAA Plasmadynamics and Lasers Conference*, Chicago, IL, Jun. 28 – Jul. 1, 2010, AIAA Paper 2010-4492.

[20] Gordeyev, S., Burns, R., Jumper, E.J., Gogineni, S., and Wittich, D.J., "Aero-Optical Mitigation of Shocks Around Turrets at Transonic Speeds Using Passive Flow Control," *51st AIAA Aerospace Sciences Meeting*, Grapevine, TX, 7 - 10 January 2013**,** AIAA Paper 2013-0717.

[21] Sutton, G.W., “Effect of turbulent fluctuations in an optically active fluid medium.” *AIAA Journal*, 7(9): 1737-1743, Sept. 1969.
[22] Gordeyev, S., Jumper, E.J., and Hayden, T., "Aero-Optics of Supersonic Boundary Layers," *AIAA Journal*, 50(3), 682-690, 2012
[23] Smith, A.E., Gordeyev, S., and Jumper, E.J., "Aperture Effects on Aero-Optical Distortions Caused by Subsonic Boundary Layers," *43rd AIAA Plasmadynamics and Lasers Conference*, 25 - 28 June 2012, New Orleans, LA, AIAA Paper 2012-2986